JOURNAL OF SOLID STATE CHEMISTRY 101, 340–352 (1992)

Comparative Study of Defect Structures in Lithium Niobate with Different Compositions

N. IYI, K. KITAMURA, F. IZUMI, J. K. YAMAMOTO,* T. HAYASHI,† H. ASANO,‡ AND S. KIMURA

National Institute for Research in Inorganic Materials, Namiki 1-1, Tsukuba-shi, Ibaraki 305, Japan; †Tsukuba ASGAL Co., Ltd., Tokaidai 5-5, Tsukuba-shi, Ibaraki 300-26, Japan; and ‡Institute of Materials Science, University of Tsukuba, Tsukuba-shi, Ibaraki 305, Japan

Received September 23, 1991; in revised form May 5, 1992; accepted May 7, 1992

Structure refinements were conducted on $LiNbO_3$ crystals with four different compositions, ranging from near stoichiometric (Li/(Li + Nb) = 0.498) to highly nonstoichiometric (Li/(Li + Nb) = 0.470), by the X-ray single-crystal diffraction and the TOF neutron powder diffraction methods to clarify the major defect mechanism of $LiNbO_3$ governing its nonstoichiometry. Two models—"Li-site vacancy model" and "Nb-site vacancy model"—were chosen on the basis of density data and examined in the refinements. The former is expressed as $[Li_{1-5x}Nb_x\square_{4x}][Nb]O_3$ and the latter $[Li_{1-5x}Nb_{5x}][Nb_{1-4x}\square_{4x}]O_3$, where $\square$ denotes a vacancy. The refinement results revealed that the amount of Nb occupancy was composition-independent and that Li^+ ions were replaced by the Nb^{5+} ions, creating vacancies at the Li site. Rietveld analysis of the neutron diffraction data was consistent with the X-ray refinement. These results strongly support the Li-site vacancy model.

Introduction

Lithium niobate ($LiNbO_3$, hereafter abbreviated as LN) has a wide solid solution region extending from the stoichiometric point (Li/(Li + Nb) = 0.50) to the Nb-rich side (Li/(Li + Nb) ~ 0.47) (*1*). The congruently melting composition is known to be different from the stoichiometric composition, and it was revealed that the congruent composition existed at about 48.5–48.6 mole% of Li_2O (51.5–51.4 mole% of Nb_2O_5) (*2*). The congruently melting composition is usually chosen for the growth of single crystals by the Czochralski (CZ) method. Nb-rich LN cannot be free from some kinds of defects to maintain the charge neutrality. From the viewpoint of optical properties, the stoichiometric composition is more desirable because defects introduced in the Nb-rich composition are detrimental to the optical properties of LN. To understand and control the properties of LN, knowledge of the defect structure is indispensable.

So far several defect models have been proposed for LN. Charge compensation for nonstoichiometry in LN was first thought to be achieved by oxygen and Li vacancies (*3–5*). However, Lerner *et al.* (*1*) observed an increase in the density of the Nb-rich composition and pointed out that this result could not be interpreted by the oxygen vacancy model. To explain the increase in den-

* Present address: Materials Physics Laboratory, Mitsui Mining and Smelting Co. Ltd., 1333-2 Haraichi, Ageo, Saitama 362, Japan.

0022-4596/92 $5.00

sity, they proposed another defect model in which excess Nb ions occupy the Li site. The formula they proposed was $[Li_{1-5x}Nb_x \square_{4x}]NbO_3$, where the vacancy ($\square$) was situated at the Li site (Li-site vacancy type). This cation substitution model was supported by electrical conductivity data (*6, 7*). Later, Peterson and Carnevale (*8*) proposed another kind of cation substitution model having a formula $[Li_{1-5x}Nb_{5x}][Nb_{1-4x} \square_{4x}]O_3$ on the basis of their NMR study. In their model the vacancy does not exist at the Li site but at the Nb site (Nb-site vacancy type).

Structure analysis has been done by several researchers (*9, 10*), but the first defect analysis was conducted by Abrahams and Marsh (*11*) by the single crystal X-ray diffraction method in 1986. Their careful refinement on the data of well-characterized stoichiometric and congruent LN crystals resulted in the structure parameters which were in excellent agreement with the Nb-site vacancy type model. The formula $[Li_{1-5x}Nb_{5x}]Nb_{1-4x}O_3$, where $x = 0.118(7)$, was given for the congruent LN composition as the result. Later, on energetic grounds, Donnerberg *et al.* (*12*) pointed out that the Nb-site vacancy type defect is far more unfavorable than the Li-site vacancy type; however, they considered that the microscopic ilmenite-like stacking could overcome the energy difference as much as 6 eV per Li_2O, though no quantitative data for this assumption were given (*12, 13*). At present, this Nb-site vacancy model is generally accepted and defect chemistry such as the effect of dopants has been discussed on the basis of this model (*14–17*).

In the field of single crystal growth of LN, the new traveling solvent FZ (floating zone) technique, using a Pt melt suspender, was successfully developed by Kitamura *et al.* (*18*) to control the nonstoichiometry of LN. In the course of diffusion studies of the resulting crystals of different nonstoichiometries (*19, 20*), questions arose on the accepted defect structure model of LN. It was observed that the diffusion rate of ions such as Ti^{4+} which was thought to occupy the Nb site exhibited no dependency on nonstoichiometry. This result was not consistent with the generally accepted idea of "vacancy at the Nb site."

In the present study, the structure of LN crystals of four different compositions grown from the melt by the FZ and CZ methods was examined by the X-ray single-crystal diffraction method and the neutron powder diffraction method. The aim of this paper is to reexamine the major defect structure of LN governing the nonstoichiometry. The defects due to reduction and minor point defects are not within the realm of this study.

Sample Preparation

The single crystals of different compositions for X-ray and neutron diffraction experiments were grown by melt growth techniques. Except for the congruent LN, which was grown by the CZ method, single crystals were grown by the FZ method. The FZ apparatus is equipped with an ellipsoidal mirror, and infrared radiation generated by a halogen lamp was used as the heat source (Nichiden Co., Ltd.). Li_2CO_3 (Kojyundo Co., Ltd., 99.9%) and Nb_2O_5 (Kojyundo Co., Ltd., 99.99%) powders were mixed in the proper amounts in an agate mortar. They were ball-milled in ethanol, dried, and calcined. Charge rods were made from the prereacted powder using a cold isostatic press, followed by a final sintering at about 1000°C in an oxygen atmosphere. To maintain the compositional homogeneity in the grown crystals, the molten zone, which was supported by the Pt heat suspender, was adjusted to the composition in equilibrium with the solid composition. The growth rate was 1.0 mm/hr and the growth atmosphere was air. The CZ-growth congruent LN was obtained from Tsukuba ASGAL Co., Ltd.

Composition and Characterization

Single crystals of LN of four different compositions were prepared. The obtained boules were characterized by chemical analysis and measurements of Curie temperatures, densities, and lattice parameters.

Chemical analysis was conducted as follows. The crushed samples were dissolved with HNO_3-HF solution in a closed Teflon vessel at 150°C overnight. The resulting solution was passed through an anion exchanger (SA-1) to separate Li and Nb ions. The Li content was measured by atomic absorption analysis of the effluent. Nb ions eliminated from the resin by HCl-HF solution were precipitated by Cuperon, and the precipitate was dried and incinerated. Weighing of the yielded Nb_2O_5 gave the Nb content.

The Curie temperature was determined by differential thermal analysis (DTA) using a TAS 7000 apparatus (Rigaku Co., Ltd) under ambient atmosphere (*21*) with a reference standard, α-Al_2O_3. The heating and cooling rate was 20°C/min.

The density was measured by the method of Archimedes using highly pure water (ion-exchanged, Millipore-filtered, and degassed under vacuum; resistivity > 17 MΩ/cm) as the medium. The LN samples were cut in a rectangle shape and the faces were polished. The accuracy of the measurement was checked by the density measurement of an α-Al_2O_3 single crystal (d_{meas} (27°C) = 3.9882(3) g/cm^3 compared with the calculated value of 3.9885 g/cm^3).

The lattice parameters were calculated from the 2θ data obtained on an X-ray powder diffractometer (Phillips PW1700) using Cu$K\alpha_1$ radiation (λ = 1.5405 Å). An internal silicon standard was used, and the lattice parameters were calculated by the least-squares method using 34 reflections in the range 2θ = 48°–138°. The lattice parameters were also obtained on single crystals mounted on a computer-controlled four-circle diffractometer (AFC-3, Rigaku Co., Ltd.), which was calibrated using a tiny single crystal Si sphere as the standard. The lattice parameters obtained on the basis of 2θ values (24 reflections, $65° < 2\theta < 90°$, Mo$K\alpha_1$ radiation) were well consistent with the data obtained by the powder diffraction method (Table I). The lattice parameters of ST and CG are also in good agreement with the result of Redfield and Burke (*22*; for review of the lattice parameters, see Ref. *23*). Abbreviations and data of the samples are given in Table I. Error values in parentheses without a decimal point correspond to the least significant digit in the function values.

Structure Refinements

1. Four-Circle X-Ray Diffraction

Structure refinements were carried out for these LN single crystals after poling. The X-ray (precession and Weisenberg) photos and electron diffraction (Hitachi H-500, with an accelerating voltage of 100 kV) confirmed the space group $R3c$. No sign of superstructure was found. Specimens were cut into rectangular crystals, which were further ground to spheres. The resulting spherical crystals (with a diameter of 0.124(6) mm for ST, 0.140(3) mm for CG, 0.110(8) mm for HN) were mounted on the AFC-3 automatic four-circle diffractometer. Intensity was measured using graphite monochromatized Mo$K\alpha$ radiation (λ = 0.71068 Å) in a ω-2θ scanning mode up to 2θ = 120°. The scanning speed was 1° min^{-1} in ω. All reflections with $-h + k + l = 3n$ for hkl and $l = 2n$ for hhl (in the hexagonal expression) of six asymmetric units were collected, to which Lorenz polarization and absorption corrections were applied. Linear absorption coefficients were 54.29 (ST), 54.61 (CG), and 55.02 (HN) cm^{-1}. Since the maximum and minimum absorption correction factors were 1.681 and 1.576 for ST, 1.775 and 1.675 for CG, and 1.614 and 1.501 for HN, absorption due to the crystal shape

TABLE I

CRYSTALLOGRAPHIC DATA

Specimen	ST	CG	MN	HN
Composition Li/(Li + Nb)	0.498(2)	0.485(2)	0.475(2)	0.470(2)
Curie temperature (K)	1467	1418	1376	1358
Space group	*R*3*c*	*R*3*c*	*R*3*c*	*R*3*c*
Lattice parameters (Å)[a]				
a	5.1482(1)	5.1499(2)	5.1515(1)	5.1525(3)
c	13.857(1)	13.864(1)	13.874(1)	13.873(1)
Lattice parameters (Å)[b]				
a	5.1485(1)	5.1499(1)	5.1523(2)	5.1525(1)
c	13.8581(4)	13.8647(4)	13.8728(6)	13.8722(4)
V (Å^3)	318.06	318.43	318.86	318.96
F (000)	408.19	409.53	410.51	411.00
M_r	147.918	148.416	148.782	148.963
Z	6	6	6	6
D_{meas} (g/cm^3)	4.637(4)	4.645(4)	—	4.652(4)
D_{calc} (g/cm^3)[c]	4.6335	4.6437	4.6489	4.6531

[a] In the hexagonal expression. Obtained by the X-ray powder diffraction method.
[b] Obtained from the single-crystal X-ray data on the four-circle diffractometer.
[c] Calculated from the obtained cell volume (V) and the formula of the cation-substitution model.

was also corrected by applying the algorithm of Busing and Levy (*24*). A set of four standard reflections was used for monitoring the fluctuation of the source X-ray intensity. No systematic intensity change was observed for ST and HN. CG data were corrected for minor intensity fluctuation. The errors of the mean F for a group of the six symmetry-equivalent reflections were calculated from (i) the σF_c's based on counting statistics corrected for the absorption error and variation in the standards (*25, 26*) and (ii) the deviations of the single measurement from the mean (σF_m). The larger of the two for each reflection was used (*27, 28*) as the weighing factor in the least-squares refinement ($w = 1/(\sigma F)^2$). Averaging of the equivalent reflections and omission of the reflections with $I < 4\,\sigma I$ gave the final sets of nonzero independent reflections (a total of 984 for ST, 948 for CG, 903 for HN). Internal agreement factors within equivalent reflections ($R_{int} = \Sigma|F - \langle F\rangle|/\Sigma|F|$ and $wR_{int} = (\Sigma w(F - \langle F\rangle)^2/\Sigma w|F|^2)^{1/2}$) were 0.0077 and 0.0076 for ST, 0.0069 and 0.0070 for CG, and 0.0091 and 0.0087 for HN, respectively.

For the refinement, the neutral and ionic scattering factors were taken from Ref. (*29*), and the values for $O^{1/3-}$ was obtained by interpolation. Two scattering factor sets, (Li^0, Nb^0, O^0) and (Li^{1+}, Nb^0, $O^{1/3-}$), were considered. Anomalous dispersion correction ($\Delta f'$ and $\Delta f''$) for Nb and O (*29*) was included in the refinement. The full-matrix least-squares program used was a modified RSFLS-4 (*30*), and Fourier synthesis were done using RSSFR-5 (*31*). As the initial parameters for refinement, reported atomic coordinates (*11*) were used with appropriate isotropic temperature factors. Least-squares refinement was continued until the maximum parameter shift (Δ/σ) $< 1.0 \times 10^{-2}$. Values for significance tests on the wR-factor ratio ($\mathcal{R}$, Hamilton's ratio) were taken from Refs. (*29, 32*).

All data were corrected for secondary extinction using the algorithm of Becker and Coppens (*33, 34*). Two extinction parame-

ters, g (mosaic distribution) and r (spherulite radius), were included in the refinement. Anharmonicity in thermal motion was also investigated by incorporating the Gram–Charlier expansion up to fourth rank tensors (*35*) in the least-squares program, since the anharmonicity is known to influence occupancy (*36*). The site symmetry restrictions were from (*29*).

2. *Neutron Powder Diffraction*

Neutron diffraction data were taken on a time-of-flight (TOF) neutron powder diffractometer, HRP (*37*), at the KENS pulsed spallation neutron source at the National Laboratory for High Energy Physics (KEK) in Japan. The samples, ST, CG, and MN, were crushed into fine powder in an agate mortar. Each batch of powder specimen was loaded into a cylindrical vanadium cell 5 mm in radius, 42 mm in height, and 25 μm in thickness, and placed in an Al vacuum chamber. The cell was turned around its axis during data collection. Intensity data were measured at room temperature using 12 ^{3}He counters installed with an average scattering angle, 2θ, of 170° and then time-focused by off-line data processing. The dependence of the incident intensity on TOF was monitored during data collection with a fission chamber. This spectrum was smoothed by a combination of Fourier transform, low-pass filtering, and inverse Fourier transform.

The refinements of the structures were accomplished by the Rietveld method (*38*), using the computer program RIETAN for TOF neutron diffraction (*39*). Intensity data corresponding to lattice plane spacings, d, between 0.0506 and 0.290 nm were used for the refinements. The values of coherent scattering lengths used for the Rietveld analysis were -1.900 fm for Li, 7.054 fm for Nb, and 5.803 fm for O (*40*). A reflection was regarded as contributing to a profile up to a point for which the ratio (intensity of the reflection at the point)/(peak height) was

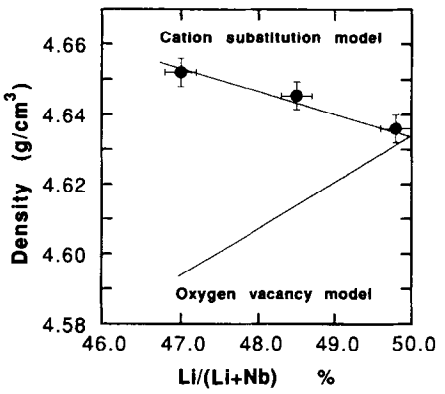

FIG. 1. Measured and calculated densities of $LiNbO_3$ as a function of composition.

0.0025. Preferred orientation was not corrected for.

Defect Structure Models and Refinement Process

The three probable defect structure models so far proposed are listed below.

(i) Oxygen vacancy model

$$[Li_{1-2x}\square_{2x}][Nb][O_{3-x}\square_x]$$

(ii) Cation substitution models,

(a) Li site vacancy model

$$[Li_{1-5x}Nb_x\square_{4x}][Nb]O_3$$

(b) Nb-site vacancy model

$$[Li_{1-5x}Nb_{5x}][Nb_{1-4x}\square_{4x}]O_3$$

Increase of the density as the Li_2O content decreases was reported (*1, 11, 41, 42*). The present study confirmed it and the obtained densities were found to be compatible with the theoretical density for cation substitution models (a) and (b), but not with the oxygen vacancy model (Table I, Fig. 1). Here, the difference between cation substitution models (a) and (b) exist in the vacancy site, not in density. Oxygen vacancies, if they exist, may play only a minor role in LN nonstoichiometry, so oxygen vacancy was not considered in the refinement; namely, the occupancy of oxygen was fixed at 100% in the refinement process. The cation substi-

TABLE II

THEORETICAL FORMULAE FOR THE TWO CATION-SUBSTITUTION MODELS

Li/(Li + Nb)	Specimen	Formula[a]	
		Li-site vacancy model	Nb-site vacancy model
0.500	—	$[Li_{1.0}][Nb_{1.0}]O_3$	$[Li_{1.0}][Nb_{1.0}]O_3$
0.498	ST	$[Li_{0.994}Nb_{0.0013}\square_{0.004}][Nb]O_3$	$[Li_{0.994}Nb_{0.006}][Nb_{0.996}\square_{0.004}]O_3$
0.485	CG	$[Li_{0.951}Nb_{0.0098}\square_{0.039}][Nb]O_3$	$[Li_{0.951}Nb_{0.049}][Nb_{0.961}\square_{0.039}]O_3$
0.475	MN	$[Li_{0.919}Nb_{0.0161}\square_{0.065}][Nb]O_3$	$[Li_{0.919}Nb_{0.081}][Nb_{0.935}\square_{0.065}]O_3$
0.470	HN	$[Li_{0.904}Nb_{0.0192}\square_{0.077}][Nb]O_3$	$[Li_{0.904}Nb_{0.096}][Nb_{0.923}\square_{0.077}]O_3$

[a] $\square$ denotes a vacancy.

tution models assume the presence of Nb at the Li site (Nb_{Li}); hence Nb_{Li} was included in the final stage of refinement. Table II lists the theoretical formulae of the models for the LN of the different compositions we prepared.

Under these preconditions, our refinement was conducted as follows.

(i) Refinement of the undefected stoichiometric LN structure for clarifying refinement conditions such as the scattering factor set to obtain reasonable results. Confirmation of the results by the neutron powder diffraction method.

(ii) Application of the same refinement conditions to the other LN compositions.

(iii) Final refinement under the constraint of composition (Li/Nb ratio).

(iv) Final test of the defect model by the neutron powder diffraction method.

Results of Structure Refinement

1. Stoichiometric LN (ST)

Isotropic refinement converged successfully to $R = \Sigma||F_0| - |F_c||/\Sigma|F_0| = 4.13\%$, $wR = (\Sigma w(|F_0| - |F_c|)^2/\Sigma|F_0|^2)^{1/2} = 4.83\%$, $S = [\Sigma w(|F_0| - |F_c|)^2/(m - n)]^{1/2} = 5.27$. As the large F_c's were systematically larger than F_0's, an extinction correction was introduced. The refinement was conducted using the scattering factor set (Li^0, Nb^0, O^0). Refinement including secondary extinction led to $R = 1.47\%$, $wR = 1.80\%$, $S = 1.97$. Anisotropic refinement incorporating anharmonic thermal motion was successively conducted with varied occupation factors at the Li and Nb sites, yielding the formula $[Li_{1.04(5)}][Nb_{0.997(3)}]O_3$ with $R = 0.62$, $wR = 0.89$, and $S = 0.975$. The ratio wR (harmonic)/wR (anharmonic) = 1.067, which is $> \mathcal{R}_{9,954,0.005} = 1.012$, indicated that significant improvement at the 0.5% level was attained by incorporation of anharmonic thermal vibration. Here Nb at the Nb site was the only atom in which anharmonicity was introduced. It was (i) because refinement was not conducted successfully for more than two atoms with anharmonic thermal motion tensors and (ii) because a shift of the electron density could be expected most for the Nb due to its covalency. The partially ionic scattering factor set (Li^{1+}, Nb^0, $O^{1/3-}$) resulted in a similar formula, $[Li_{1.04(5)}][Nb_{0.995(3)}]O_3$, with essentially the same R factors. Considering the Nb occupancy, the neutral scattering factor set (Li^0, Nb^0, O^0) was chosen. For extinction correction, the Lorentzian mosaic distribution was assumed (*33, 34*) since it always gave significantly lower wR values than the Gaussian distribution.

The distribution of Li and Nb between

TABLE III

THE POSITIONAL AND THERMAL PARAMETERS OF $LiNbO_3$ CRYSTALS OBTAINED BY THE X-RAY SINGLE-CRYSTAL DIFFRACTION METHOD

Atom	Site	Sample	Positional parameters			Thermal parameters[a] ($\times 10^5$)						B_{eq}[b]
			x	y	z	U_{11}	U_{22}	U_{33}	U_{12}	U_{13}	U_{12}	
Li	6*a*	ST	0	0	0.2802(5)	1460(162)	U_{11}	2054(174)	$\frac{1}{2}U_{11}$	0	0	1.31
		CG	0	0	0.2795(4)	1100(157)	U_{11}	1490(151)	$\frac{1}{2}U_{11}$	0	0	0.97
		HN	0	0	0.2814(4)	990(156)	U_{11}	1129(151)	$\frac{1}{2}U_{11}$	0	0	0.82
Nb	6*a*	ST	0	0	0	466(12)	U_{11}	400(8)	$\frac{1}{2}U_{11}$	0	0	0.350
		CG	0	0	0	605(14)	U_{11}	387(12)	$\frac{1}{2}U_{11}$	0	0	0.420
		HN	0	0	0	707(14)	U_{11}	646(11)	$\frac{1}{2}U_{11}$	0	0	0.542
O	18*b*	ST	0.04775(10)	0.3432(2)	0.0637(3)	743(12)	588(11)	715(8)	337(11)	−112(11)	−211(9)	0.537
		CG	0.04818(11)	0.3431(2)	0.0627(2)	791(13)	611(12)	775(8)	350(12)	−137(12)	−244(9)	0.574
		HN	0.04850(14)	0.3432(2)	0.0644(3)	838(16)	633(15)	849(11)	360(17)	−148(14)	−250(12)	0.613

[a] The temperature factor is expressed as $\exp(-2\pi^2(h^2a^{*2}U_{11} + k^2b^{*2}U_{22} + l^2c^{*2}U_{33} + 2hka^*b^*U_{12} + 2hla^*c^*U_{13} + 2klb^*c^*U_{23})$.
[b] $B_{eq} = \frac{4}{3}(\Sigma_i\Sigma_j B_{ij}a_ia_j) = \frac{8}{3}\pi^2(\Sigma_i\Sigma_j U_{ij})$.

the Nb and Li sites was further investigated since the ST specimen was not strictly stoichiometric. The compositional constraint Li/Nb = 0.99203 was imposed in the final refinement. Under the constraint, the formula $[Li_{0.996(3)}Nb_{0.005(2)}]Nb_{0.999(3)}O_3$ resulted, where the anisotropic thermal parameters of Li were used for Nb_{Li}. The corresponding indicators were $R = 0.61\%$, $wR = 0.89\%$, $S = 0.98$, respectively. The validity of the weight assignment was investigated: a normal probability δR plot (*27*) showed a near linear line with a slope of 0.7 and with zero intercept, and at the 1% confidence level, the range of the accuracy indicator $U_{0.01}$ (defined in Ref. *26*) was 1.030 ~ 0.927. These values indicate the correctness of the weighting system and the absence of apparent systematic errors. The final wR was larger than the intrinsic accuracy of the measurement wR_{int}, which assures validity of the refinement result. The obtained formula are in good agreement with the Li-site vacancy model.

The positional parameters and thermal parameters corresponding to the final refinement are given in Table III, and the bond lengths and angles are given in Tables IV and V, respectively. The extinction correction parameters were $g = 1.02(3) \times 10^4$ and $r = 5.5(3)$ μm. Two factors, $d_{1111} = 4.7(9) \times 10^{-6}$ and $d_{1133} = 0.16(3) \times 10^{-6}$, were greater than 4 e.s.d. of the nine independent higher order coefficients. The difference Fourier maps gave residual electron densities ranging from +0.33 e/Å^3 (0.1, 0.1, 0.0) to −0.60 e/Å^3 (0.0, 0.0, 0.04). The residual electron density was +0.08 e/Å^3 at the

TABLE IV

THE BOND ANGLE

Bond		ST	CG	HN
O–Li–O[a]	(1)	109.33(17)	109.23(14)	109.14(15)
	(2)	80.84(7)	80.85(6)	80.86(6)
	(3)	89.34(8)	89.43(6)	89.50(7)
	(4)	153.13(28)	153.28(23)	153.40(25)
	(5)	74.34(18)	74.44(15)	74.51(16)
O–Nb–O[b]	(1)	79.91(10)	79.46(8)	80.13(9)
	(2)	88.63(3)	88.55(2)	88.75(3)
	(3)	90.02(3)	89.93(2)	90.13(2)
	(4)	165.86(16)	165.21(12)	166.28(14)
	(5)	99.71(12)	100.15(9)	99.36(10)

[a] The angles are in the order: $z + \frac{1}{6}$ to $z + \frac{1}{6}$, $z + \frac{1}{6}$ to $z + \frac{1}{3}$, $z + \frac{1}{6}$ to $z + \frac{1}{3}$, $z + \frac{1}{6}$ to $z + \frac{1}{3}$, and $z + \frac{1}{3}$ to $z + \frac{1}{3}$. Here $z = z$ coordinate of O in Table III. The unit is the degree (°).

[b] The angles are in the order: $z - \frac{1}{6}$ to $z - \frac{1}{6}$, $z - \frac{1}{6}$ to z, $z - \frac{1}{6}$ to z, $z - \frac{1}{6}$ to z, and z to z. Here $z = z$ coordinate of independent O in Table III. The unit is the degree (°).

TABLE V
THE BOND LENGTH

Bond	z coordinate[a]	Number	Bond length (Å) ST	CG	HN
Li–O	$z + \frac{1}{6}$	3	2.056(3)	2.061(2)	2.065(3)
O′	$z + \frac{1}{3}$	3	2.260(5)	2.258(4)	2.255(5)
Nb–O	z	3	1.878(2)	1.871(2)	1.883(2)
O′	$z - \frac{1}{6}$	3	2.127(3)	2.137(2)	2.121(3)
Li–Nb	$z + \frac{1}{2}$	1	3.046(6)	3.057(5)	3.032(6)
Nb′	$z + \frac{1}{3}$	3	3.062(2)	3.066(2)	3.061(2)
Nb″	$z + \frac{1}{6}$	3	3.363(3)	3.360(3)	3.374(3)

[a] The z coordinates of the right-side atoms are listed. z, the z coordination of the independent atoms in Table III.

Li site, $+0.25$ e/Å^3 at the Nb site, and $+0.12$ e/Å^3 at the O site. The polarity sense was examined by refining the model with all hkl's replaced with the Friedel pairs $\bar{h}\bar{k}\bar{l}$'s. The ratio of $wR(\bar{h}\bar{k}\bar{l})/wR(hkl)$ was found to be 1.44, which confirmed the polarity of the refined atomic parameters since the Hamilton's ratio $\mathcal{R}_{1.954,0.005} = 1.0041$. The same refinement procedure was applied in the refinement of the other LN crystals of different composition.

This structure of ST was confirmed by the powder neutron diffraction method. Since the Nb_{Li} and vacancies were negligible, the stoichiometric formula $LiNbO_3$ was assumed in the refinement. The anisotropic refinement was conducted using the parameters obtained by the X-ray refinement. The R factors were $R_{wp} = 4.39\%$, $R_p = 3.33\%$, $R_e = 3.96\%$, $R_I = 1.63\%$, and $R_F = 0.84\%$. The resulting parameters are given in Table VI. The occupation factors of Li and Nb were varied, and the obtained values were 1.095(25) and 0.996(6) for each site. These occupancies were consistent with the X-ray result.

2. Congruent LN (CG)

The first isotropic refinement resulted in $R = 4.71\%$, $wR = 4.81\%$, and $S = 5.42$, leaving many of large F's much smaller than the calculated ones. The secondary extinction correction improved the indicators considerably, yielding $R = 2.12\%$, $wR = 2.59\%$, and $S = 2.91$. For investigation of the distribution of the Li and Nb, Nb_{Li} was included. Compositional constraint Li/Nb = 0.94175 resulted in $[Li_{0.934(4)}Nb_{0.008(3)}]$-$Nb_{0.984(4)}O_3$ with indicators $R = 0.76\%$, $wR = 0.95\%$, and $S = 1.07$. Here anharmonicity was included and the obtained ratio wR (harmonic)/wR (anharmonic) = 1.28 assured significant improvement. At the 1% confidence level the range of $U_{0.01}$ was 1.13 ~ 1.01. A normal probability δR plot with a slope of about 0.8 with zero intercept indicated the appropriateness of the weight estimation and the absence of apparent systematic error. The relation $wR > wR_{int}$ assures the validity of the final result. The obtained formulae are in agreement with the Li-site vacancy model.

The positional and thermal parameters under the compositional constraint are given in Table III, and the bond lengths and angles are given in Tables IV and V, respectively. The extinction parameters, g and r, were $1.07(4) \times 10^4$ and 6.1(4) μm, respectively. Four coefficients, $c_{333} = 1.3(1) \times 10^{-5}$, $d_{1111} = 1.0(1) \times 10^{-5}$, $d_{1133} =$

TABLE VI

POSITIONAL AND THERMAL PARAMETERS OBTAINED BY THE NEUTRON POWDER DIFFRACTION METHOD[a]

Atom	Site	Sample	Positional parameters			Thermal parameter
			x	y	z	B_{eq}[b]
Li	6*a*	ST	0	0	0.2803(4)	1.18
		CG	0	0	0.2809(8)	1.06
		MN	0	0	0.2802(5)	0.98
Nb	6*a*	ST	0	0	0	0.437
		CG	0	0	0	0.424
		MN	0	0	0	0.531
O	18*b*	ST	0.0472(3)	0.3423(4)	0.0633(1)	0.690
		CG	0.0481(4)	0.3433(6)	0.0638(2)	0.547
		MN	0.0480(3)	0.3423(4)	0.0641(2)	0.685

[a] Lerner-type formula was assumed in the Rietveld refinement. Occupancies were fixed.
[b] $B_{eq} = \frac{4}{3}(\Sigma_i\Sigma_j B_{ij}\boldsymbol{a}_i\boldsymbol{a}_j) = \frac{8}{3}\pi^2(\Sigma_i\Sigma_j U_{ij})$.

$2.2(5) \times 10^{-7}$, and $d_{1123} = -5.1(4) \times 10^{-7}$, were greater than 4 e.s.d. of the nine independent higher order coefficients. The maximum residual electron density, $\Delta\rho_{max}$, in the final difference Fourier maps was $+0.50$ e/Å^3 (0.0, 0.0, 0.0), and the minimum residual electron density, $\Delta\rho_{min}$, -0.74 e/Å^3 (0.0, 0.0, 0.05). The residual electron density was $+0.17$ e/Å^3 at the Li site, $+0.50$ e/Å^3 at the Nb site, and -0.10 e/Å^3 at the O site. The refinement using $F(\bar{h}\bar{k}\bar{l})$ yielded the factors $R = 1.12$, $wR = 1.38$, and $S = 1.56$. Polarity assignment was confirmed from the ratio $wR(\bar{h}\bar{k}\bar{l})/wR(hkl) = 1.45$, compared with $\mathcal{R}_{1,920,0.005} = 1.0042$.

Neutron Rietveld analysis was conducted on the congruent LN on the basis of the two defect models. When the Li-site vacancy model was assumed with the compositional constraint (Li/Nb ratio), anisotropic refinement was successfully accomplished, giving good indicators, $R_{wp} = 5.00\%$, $R_p = 3.82\%$, $R_e = 3.60\%$, $R_I = 3.32\%$, and $R_F = 1.68\%$ with $\chi^2 = 1.924$. The obtained positional and thermal parameters were reasonable. On the contrary, under the Nb-site vacancy model, the R factors worsened significantly. The R factors were $R_{wp} = 5.43\%$, $R_p = 4.12\%$, $R_e = 3.60\%$, $R_I = 3.46\%$, and $R_F = 1.73\%$ ($\chi^2 = 2.272$) and the U_{11} thermal parameter at the Li site became negative ($U_{11} = -0.0018(22)$). The final parameters obtained are given in Table VI.

3. *Nonstoichiometric LN (MN)*

An LN single crystal with Li/(Li + Nb) = 0.475 was used for the neutron powder diffraction. The two defect models were assumed in the anisotropic Rietveld refinement and results were compared. Under the constraint of the Lerner formalism, the R factors were successfully reduced to $R_{wp} = 4.42\%$, $R_p = 3.41\%$, $R_I = 2.27\%$, $R_F = 1.15\%$, and $\chi^2 = 1.297$ with reasonable positional and anisotropic thermal parameters (e.g., for the Li site, $B_{eq} = 0.977$ Å^2, $U_{11} = 0.0070(16)$ Å^2, and $U_{33} = 0.021(5)$ Å^2). In contrast, in the Nb-site vacancy model, the U_{11} temperature factor at the Li site was shifted to a more negative value ($-0.0034(19)$ Å^2). The B_{eq} (Å^2) of Li was also as small as 0.117. The R factors obtained were $R_{wp} = 4.89\%$, $R_p = 3.74\%$, $R_I = 2.75\%$, and $R_F = 1.40\%$ ($\chi^2 = 1.591$), which are significantly worse than those obtained in the Li-site vacancy model. The

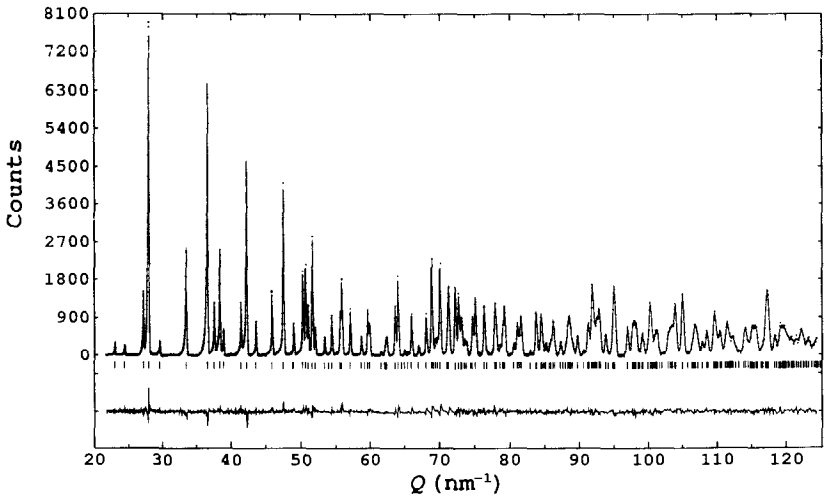

FIG. 2. Rietveld refinement patterns for sample MN plotted against $Q (= 2\pi/d)$. Dots show observed neutron intensities, and the solid line represents calculated intensities. The difference between the observed and the calculated intensities is depicted at the bottom in the same scale.

negative thermal parameters imply excess positive nuclear scattering at the Li site, which is consistent with the Li-site vacancy model. The final profile fit and difference patterns corresponding to the Li-site vacancy model are given in Fig. 2, and the positional and thermal parameters are given in Table VI.

4. Nonstoichiometric LN (HN)

The isotropic least-squares refinement resulted in $R = 3.79\%$, $wR = 4.21\%$, and $S = 3.99$. Inclusion of the secondary extinction correction improved the agreement factors markedly to $R = 2.17\%$, $wR = 2.66\%$, and $S = 2.52$. Anisotropic refinement including anharmonic tensors as well as Nb_{Li} was then conducted. Imposition of the compositional constraint, Li/Nb = 0.8868, resulted in a formula, $[Li_{0.891(4)}Nb_{0.013(2)}]Nb_{0.992(4)}O_3$, with indicators $R = 0.71\%$, $wR = 1.04\%$, and $S = 0.98$. The ratio wR (harmonic)/wR (anharmonic) = $1.39 > \mathcal{R}_{1.875,0.005} = 1.0045$; hence the improvement was significant at the 0.5% level. The yielded formula was consistent with the expected Li-site vacancy formula, $[Li_{0.904}Nb_{0.0192}][Nb]O_3$.

The positional parameters and thermal parameters corresponding to the final refinement are given in Table III, and bond lengths and angles are given in Tables IV and V, respectively. The final extinction correction factors were $g = 0.50(2) \times 10^4$ and $r = 40\ (32)\ \mu m$. Four parameters, $d_{1111} = 8.9(12) \times 10^{-6}$, $d_{3333} = 1.2(2) \times 10^{-7}$, $d_{1133} = 5.1(6) \times 10^{-7}$, and $d_{1123} = -6.5(5) \times 10^{-7}$, were greater than 4 e.s.d. of the nine independent higher order coefficients. The residual electron density in the final difference Fourier maps was in the range $+0.56$ e/Å^3 (0.0, 0.0, 0.04) to -0.56 e/Å^3 (0.05, 0.70, 0.70) with $+0.17$ e/Å^3 at the Li site, $+0.16$ e/Å^3 at the Nb site, and $+0.01$ e/Å^3 at the O site. The polarity of the refined parameters was confirmed by the ratio $wR(\bar{h}\bar{k}\bar{l})/wR(hkl) = 1.44$.

Defect Structure of LN

The formulae obtained in the present study are listed in Table VII. To summarize,

TABLE VII

FORMULAE OBTAINED BY X-RAY REFINEMENT

Specimen	Formula: Expected (Li-site vacancy model)	Formula: Obtained[a]
ST	$[Li_{0.994}Nb_{0.0013}]NbO_3$	$[Li_{0.996(3)}Nb_{0.005(2)}]Nb_{0.999(3)}O_3$
CG	$[Li_{0.951}Nb_{0.0098}]NbO_3$	$[Li_{0.934(4)}Nb_{0.008(2)}]Nb_{0.984(4)}O_3$
HN	$[Li_{0.904}Nb_{0.0192}]NbO_3$	$[Li_{0.891(4)}Nb_{0.013(2)}]Nb_{0.992(4)}O_3$

[a] The formulae obtained correspond to the final anharmonic refinement under the constraint of composition (Li/Nb ratio).

our X-ray and powder neutron results were consistent with the Li-site vacancy model, or Lerner's model, contrary to the refinement by Abrahams and Marsh (*11*). Our results are also consistent with the results of the energy calculation for isolated defects by Donnerberg *et al.* (*12*).

Even by the single-crystal X-ray method, it is difficult to obtain precise occupation parameters at the cation sites of LN due to the facts that (i) low scattering factors of Li compared with Nb make information on Li uncertain and (ii) the correction of extinction and anharmonic thermal motion, and choice of scattering factor table affect the final occupation factors. In the present study, to avoid these problems, the same refinement process, which had been checked on the defect-free LN or stoichiometric LN, was applied to all LN samples prepared by essentially the same synthetic method. To avoid the problems of extinction, valency, etc., the X-ray result was complimented by the neutron powder diffraction method. The advantages of neutron diffraction method are as follows. Neutron nuclear scattering lengths for Li and Nb are in the same order and independent of valency; furthermore, the opposite sign in the scattering lengths (-1.900 fm for Li, 7.054 fm for Nb) can emphasize the occupancy differences at the Li site between the two models. Indeed the powder diffraction method is less powerful in revealing the structure than the neutron single-crystal diffraction method, but the powder method was adopted in the present study because the single-crystal diffraction method is not free from an extremely large extinction effect.

These points were not thoroughly examined in the work of Abrahams and Marsh (*11*): In their refinement, the occupancy was varied only in congruent LN, but not in stoichiometric LN. As for the preparation method, stoichiometric LN was made by the ion-diffusion method, whereas the congruent LN was from the melt (by the CZ method). No accounts of the effect of anharmonicity on the occupancy were given, though anharmonicity motion was observed in their refinement of congruent LN. Discrepancy between their results and ours may stem from these differences.

Another possible explanation for the discrepancy is the presence of a small amount of anti-site defects between Li and Nb in the congruent sample they used, which makes the Nb site apparently deficient for X-ray analysis. The anti-site defect-overlapped Li-site vacancy model looks like the Nb-site vacancy model. The Lerner formula for the congruent LN is $[Li_{0.95}Nb_{0.01}][Nb]O_3$. If, for example, 4% Li–Nb anti-site defects are present, the formula becomes $[Li_{0.91}Nb_{0.05}][Nb_{0.96}Li_{0.04}]O_3$. Since Li at the Nb site cannot be detected because of its weak scattering power, this formula would be comparable with the formula $[Li_{0.941}Nb_{0.059}][Nb_{0.953}]O_3$ which they reported. The concentration of the Li–Nb anti-site defects may vary according to the crystal growth conditions. Their stoichiometric LN was prepared by Li ion diffusion, which may have changed the concentration of Li–Nb anti-site defects. In any case they did not vary the Li and Nb occupancies in the least-squares refinement of the stoichiometric sample as pointed out before, so it is only a possibility.

TABLE VIII

POSITIONAL AND THERMAL PARAMETERS OBTAINED BY THE X-RAY SINGLE-CRYSTAL DIFFRACTION METHOD USING THE HARMONIC VIBRATION MODEL

Atom	Site	Sample	Positional parameters			Thermal parameter B_{eq}[a]
			x	y	z	
Li	6*a*	ST	0	0	0.2800(4)	1.10(13)
		CG	0	0	0.2808(4)	0.76(16)
		HN	0	0	0.2815(4)	0.51(13)
Nb	6*a*	ST	0	0	0	0.297(2)
		CG	0	0	0	0.346(3)
		HN	0	0	0	0.419(3)
O	18*b*	ST	0.0477(1)	0.3431(1)	0.06344(4)	0.541(9)
		CG	0.0482(2)	0.3432(2)	0.06363(5)	0.573(11)
		HN	0.0483(2)	0.3429(2)	0.06397(6)	0.622(15)

[a] $B_{eq} = \frac{4}{3}(\Sigma_i\Sigma_j B_{ij}\mathbf{a}_i\mathbf{a}_j) = \frac{8}{3}\pi^2(\Sigma_i\Sigma_j U_{ij})$.

Positional Parameters

As for the positional parameters, the X-ray refinement results are in satisfactory agreement with the neutron results. Better agreement with neutron diffraction was seen for the X-ray refinement with the harmonic vibration model (Table VIII). The parameters obtained by the harmonic vibration model were also in better agreement with those obtained by Abrahams and Marsh (*11*) in the shift of the ions due to compositional change. It was observed in Ref. (*11*) that the atomic position was defined more precisely on the basis of the refinement with the harmonic vibration model, which seems to be also the case with ours. The shift of ions due to the increase in Nb concentration is depicted in Fig. 3 on the basis of the refinement using harmonic vibration.

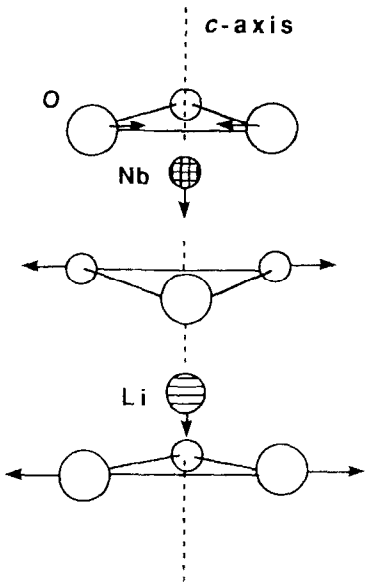

FIG. 3. The schematic representation of the shift of ions in $LiNbO_3$ as the Nb content increases. Arrows show the direction of shift, but their lengths do not correspond to the amount of the shift.

Acknowledgments

The authors are very grateful to Y. Yajima (NIRIM) for chemical analysis of the LN specimens.

References

1. P. LERNER, C. LEGRAS, AND J. P. DUMAS, *J. Cryst. Growth* **3/4,** 231 (1968).
2. J. R. CARRUTHERS, G. E. PETERSON, M. GRASSO, AND P. M. BRIDENBAUGH, *J. Appl. Phys.* **42,** 1846 (1971).
3. H. FAY, W. J. ALFORD, AND H. M. DESS, *Appl. Phys. Lett.* **12,** 89 (1968).
4. W. BOLLMANN, *Cryst. Res. Technol.* **18,** 1147 (1983).

5. K. L. SWEENEY, L. E. HALLIBURTON, D. A. BRYAN, R. R. RICE, R. GERSON, AND H. E. TOMASCHKE, *J. Appl. Phys.* **57,** 1036 (1985).
6. Y. LIMB, K. W. CHENG, AND D. M. SMITH, *Ferroelectrics* **38,** 813 (1981).
7. D. M. SMYTH, *Ferroelectrics* **50,** 93 (1983).
8. G. E. PETERSON AND A. CARNEVALE, *J. Chem. Phys.* **56,** 4848 (1972).
9. S. C. ABRAHAMS, W. C. HAMILTON, AND J. M. REDDY, *J. Phys. Chem. Solids* **27,** 1013 (1966).
10. S. C. ABRAHAMS, J. M. REDDY, AND J. L. BERNSTEIN, *J. Phys. Chem. Solids* **27,** 997 (1966).
11. S. C. ABRAHAMS AND P. MARSH, *Acta Crystallogr. Sect. B* **42,** 61 (1986).
12. H. DONNERBERG, S. M. TOMLINSON, C. R. A. CATLOW, AND O. F. SCHIRMER, *Phys. Rev. B,* **40,** 11,909 (1989).
13. D. M. SMITH, "Proceedings of the Sixth IEEE International Symposium on the Application of Ferroelectrics, June 1986."
14. W. ROSSNER, B. C. GRABMAIER, AND W. WERSING, *Ferroelectrics* **93,** 57 (1989).
15. P. K. GALLAGHER AND H. M. O'BRYAN, *J. Am. Ceram. Soc.* **71,** C-56 (1988).
16. O. F. SCHIRMER, O. THIEMANN, AND M. WÖHLECKE, *J. Phys. Chem. Solids* **52,** 185 (1991).
17. H. J. DONNERBERG, S. M. TOMLINSON, AND C. R. A. CATLOW, *J. Phys. Chem. Solids* **52,** 201 (1991).
18. K. KITAMURA, "Proceedings of the Meeting of ICCG21, Nagoya, Japan, August 1990."
19. K. KITAMURA, T. HAYASHI, T. SAWADA, N. IYI, AND S. KIMURA, "Proceedings of the 8th American Conference on Crystal Growth, Vail, Colorado, July 1990." [Abstr. No. 140].
20. K. KITAMURA, T. HAYASHI, H. HANEDA, N. IYI, AND S. KIMURA, to be published.
21. H. M. O'BRYAN, P. K. GALLAGHER, AND C. D. BRANDLE, *J. Am. Ceram. Soc.* **68,** 493 (1985).
22. D. REDFIELD AND W. J. BURKE, *J. Appl. Phys.* **45,** 4566 (1974).
23. B. C. GRABMAIER, *in* "Properties of Lithium Niobate" (EMIS Datareviews Series 5), INSPEC, p. 18 (1989).
24. W. R. BUSING AND H. A. LEVY, *Acta Crystallogr.* **10,** 180 (1957).
25. S. C. ABRAHAMS, *Acta Crystallogr.* **17,** 1327 (1964).
26. S. C. ABRAHAMS, *Acta Crystallogr. Sect. A* **25,** 165 (1969).
27. S. C. ABRAHAMS AND E. T. KEVE, *Acta Crystallogr. Sect. A* **27,** 157 (1971).
28. S. C. ABRAHAMS, J. L. BERNSTEIN, AND E. T. KEVE, *J. Appl. Cryst.* **4,** 284 (1971).
29. "International Tables for X-Ray Crystallography," Vol. 4, p. 71, Kynoch, Birmingham (1974).
30. T. SAKURAI, K. NAKATSU, H. IWASAKI, AND M. FUKUHARA, "RSFLS-4, UNICS II," The Crystallographic Society of Japan (1967).
31. T. SAKURAI, "RSSFR-5, UNICS II," The Crystallographic Society of Japan (1967).
32. W. C. HAMILTON, *Acta Crystallogr.* **18,** 502 (1965).
33. P. J. BECKER AND P. COPPENS, *Acta Crystallogr. Sect. A* **30,** 148 (1974).
34. P. J. BECKER AND P. COPPENS, *Acta Crystallogr. Sect. A* **30,** 129 (1974).
35. U. H. ZUCKER AND H. SCHULZ, *Acta Crystallogr. Sect. A* **38,** 563 (1982).
36. U. H. ZUCKER AND H. SCHULZ, *Acta Crystallogr. Sect. A* **38,** 568 (1982).
37. N. WATANABE, H. ASANO, H. ISAWA, S. SATOH, H. MURATA, K. KURAHASHI, S. TOMIYOSHI, F. IZUMI, AND K. INOUE, *Jpn. J. Appl. Phys.* **26,** 1164 (1987).
38. H. M. RIETVELD, *J. Appl. Crystallogr.* **2,** 65 (1969).
39. F. IZUMI, H. ASANO, H. MURATA, AND N. WATANABE, *J. Appl. Crystallogr.* **20,** 411 (1987).
40. V. F. SEARS, *in* "Neutron Scattering," Part A, "Methods of Experimental Physics" (K. Sköld and D. L. Price, Eds.), Vol. 23, p. 521, Academic Press, New York (1986).
41. R. J. HOLMES AND W. J. MINFORD, *Ferroelectrics* **75,** 63 (1987).
42. B. C. GRABMAIER, *in* "Properties of Lithium Niobate" (EMIS Datareviews Series 5), INSPEC, p. 24 (1989).
43. S. C. ABRAHAMS, S. K. KURTZ, AND P. B. JAMIESON, *Phys. Rev.* **172,** 551 (1968).